Rheol Acta (2013) 52:913–925
DOI 10.1007/s00397-013-0730-6

ORIGINAL CONTRIBUTION

# Slip yield stress effects in start-up Newtonian Poiseuille flows

**George Kaoullas · Georgios C. Georgiou**

Received: 30 April 2013 / Revised: 9 July 2013 / Accepted: 21 August 2013 / Published online: 17 September 2013


**Abstract** Analytical solutions are derived for various start-up Newtonian Poiseuille flows assuming that slip at the wall occurs when the wall shear stress exceeds a critical value, known as the slip yield stress. Two distinct regimes characterise the steady axisymmetric and planar flows, which are defined by a critical value of the pressure gradient. If the imposed pressure gradient is below this critical value, the classical no-slip, start-up solution holds. Otherwise, no-slip flow occurs only initially, for a finite time interval determined by a critical time, after which slip does occur. For the annular case, there is an additional intermediate (steady) flow regime where slip occurs only at the inner wall, and hence, there exist two critical values of the pressure gradient. If the applied pressure gradient exceeds both critical values, the velocity evolves initially with no-slip at both walls up to the first critical time, then with slip only along the inner wall up to the second critical time and finally with slip at both walls.

**Keywords** Newtonian fluid · Poiseuille flow · Start-up flow · Navier slip · Slip yield stress

G. Kaoullas (✉)
Oceanography Centre, University of Cyprus,
PO Box 20537, 1678 Nicosia, Cyprus
e-mail: g.kaoullas@gmail.com

G. C. Georgiou
Department of Mathematics and Statistics, University of Cyprus,
PO Box 20537, 1678 Nicosia, Cyprus
e-mail: georgios@ucy.ac.cy

## Introduction

The following are the two main macroscopic boundary conditions used at the interface between a fluid and the wall: (a) the classical no-slip condition, where the fluid is assumed to stick at the wall, and (b) the slip condition where the velocity of the fluid relative to that of the wall, known as the slip velocity, is non-zero. It is well established that under certain circumstances, even Newtonian fluids slip at walls (see Neto et al. 2005 and references therein). Various models have been developed to describe slip at the wall of both Newtonian (Neto et al. 2005; Ferrás et al. 2012) and non-Newtonian fluids (Barnes 1995; Denn 2001; Hatzikiriakos 2012; Ferrás et al. 2012). The slip velocity has been related to the wall shear stress, the wall normal stress, pressure, molecular weight and its distribution, temperature as well as to the surface roughness and the interaction between the fluid and the wall interface (Hatzikiriakos 2012; Ansari et al. 2013).

The first slip model was proposed by Navier (1827), who assumed that the wall shear stress, $\tau_w$, depends linearly on the slip velocity, $u_w$:

$$\tau_w = \beta u_w \tag{1}$$

where $\beta$ is the slip *(or friction)* coefficient, which is also defined as the ratio of the viscosity, $\eta$, to the slip or extrapolation length, $b$, i.e. the distance from the interface so that the fluid velocity extrapolates to zero. As the amount of experimental data was increasing, so did the need to develop

other slip models which could describe better experimental observations. These include non-linear as well as dynamic slip models (Hatzikiriakos 2012).

The Navier slip condition describes well certain experimental data regarding Newtonian fluids (Neto et al. 2005; Matthews and Hill 2008). However, other experiments (Craig et al. 2001; Zhu and Granick 2001, 2002; Spikes and Granick 2003; Neto et al. 2003) show that the slip length also depends on the wall shear stress. Spikes and Granick (2003) proposed a modified Navier slip model, where slip occurs only when a critical value of the wall shear stress, $\tau_c$, known as the slip yield stress, is exceeded:

$$\left.\begin{array}{ll} u_w = 0, & \tau_w \le \tau_c \\ \tau_w = \tau_c + \beta u_w, & \tau_w > \tau_c \end{array}\right\}. \tag{2}$$

This slip model describes better experimental data for Newtonian liquids obtained in oscillatory squeeze flow (Spikes and Granick 2003) and in low-friction bearing experiments (Choo et al. 2007). The existence of a critical shear stress for the onset of slip in flows of polymer melts and other complex materials is well documented (Kalika and Denn 1987; Hatzikiriakos and Dealy 1991; Denn 2001; Kalyon and Gevgilili 2003). Also, Aral and Kalyon (1994) have reported that there exists a critical time for the flow to reach steadstate in steady torsional flows of viscoplastic suspensions. However, Spikes and Granick (2003) proposed Eq. (2) for Newtonian liquids (namely tetradecane and water) and reported that the slip yield stress was quite small for lyophobic surfaces and high for lyophilic ones. They also provided two possible physical origins of the model. The first concerns models based on the enhanced mobility of molecules of liquid immediately adjacent to a non-wetting wall. The second one concerns the gas film model in which, above a critical shear stress, liquid strain close to the surface may transform small droplets of gas which collect preferentially at the non-wetted surface into an extended thin film.

The power-law analogue of Eq. (2) has also been used to describe wall slip of complex fluids, such as pastes (Estellè and Lanos 2007) and colloids (Ballesta et al. 2012). A more sophisticated slip equation with slip yield stress has been proposed by Tang and Kalyon (2008a, b) in their study of flow instabilities of polymeric fluids and suspensions.

As exemplified by Ferrás et al. (2012), analytical solutions are important to solve related industrial problems, for the assessment of computational codes used in fluid flow simulations and that they form the building blocks to the understanding of more complex solutions. The steady-state Newtonian Poiseuille flow, with Navier slip, has been solved analytically by Ebert and Sparrow (1965) for the rectangular and annular geometry and by Duan and Muzychka (2007a, b) for other non-circular geometries. Chatzimina et al. (2009) also presented semi-analytical solutions for the annular geometry with non-linear slip. Analytical solutions of the transient and periodic problems with Navier slip have been derived for the planar (Majdalani 2008), axisymmetric (King 2007; Matthews and Hill 2008; Wu et al. 2008) and annular problems (Wiwatanapataphee et al. 2009). Ferrás et al. (2012) presented solutions of Newtonian and non-Newtonian Couette and Poiseuille flows using various slip laws. Analytical steady-state solutions with slip Eq. (2) have been reported by Ballesta et al. (2012) for the flow of concentrated colloidal suspensions in a cone–plate geometry, by Spikes and Granick (2003) for Newtonian squeeze flow (using an approximate expression for the ball geometry) and by Kaoullas and Georgiou (2013) for Newtonian Poiseuille flows in various geometries.

The intention of this work is to extend previous results and give analytical solutions for transient Newtonian Poiseuille flows using the slip Eq. (2), i.e. taking into account slip yield stress effects. The solutions for the axisymmetric and planar Poiseuille flows are first provided and then those for the start-up annular Poiseuille flow are presented. Finally, the conclusions of this work are provided.

## Axisymmetric Poiseuille flow

We consider the start-up pressure-driven flow of an incompressible Newtonian fluid in a circular, infinitely long, horizontal tube of radius $R$ assuming that gravity is negligible, so that the flow is unidirectional. In cylindrical polar coordinates, the $z$-velocity component $u_z(r, t)$ satisfies

$$\rho \frac{\partial u_z}{\partial t} = G + \eta \left( \frac{\partial^2 u_z}{\partial r^2} + \frac{1}{r} \frac{\partial u_z}{\partial r} \right), \tag{3}$$

where $G \equiv (-\partial p/\partial z)$ is the pressure gradient and $\rho$ is the density. Given that

$$\tau_w = |\tau_{rz}|_{r=R} = -\eta \left. \frac{\partial u_z}{\partial r} \right|_{r=R}, \tag{4}$$

the boundary condition at the wall becomes

$$\left.\begin{array}{ll} u_w = 0, & \tau_w \le \tau_c \\ -\eta \left. \dfrac{\partial u_z}{\partial r} \right|_{r=R} = \tau_c + \beta u_w, & \tau_w > \tau_c \end{array}\right\}. \tag{5}$$

Along the axis of symmetry, the usual symmetry condition is assumed. Initially, the flow is at rest, thus $u_z(r, 0) = 0$.

In steady flow, there are two flow regimes (Kaoullas and Georgiou 2013): (1) the no-slip and (2) the slip regimes,

which are defined by a critical value of the pressure gradient for the occurrence of slip:

$$G_c \equiv \frac{2\tau_c}{R}. \tag{6}$$

The steady-state velocity profile is therefore given by

$$u_z^s(r) = \begin{cases} \dfrac{R^2 G}{4\eta}\left[1-\left(\dfrac{r}{R}\right)^2\right], & G \le G_c, \\ \dfrac{R^2 G}{4\eta}\left[1+2B-\left(\dfrac{r}{R}\right)^2\right]-\dfrac{\tau_c B R}{\eta}, & G > G_c, \end{cases} \tag{7}$$

where

$$B \equiv \frac{\eta}{\beta R} \tag{8}$$

is the dimensionless inverse slip number (when $B = 0$, the no-slip case is recovered, while $B \to \infty$ corresponds to full slip).

In the start-up flow problem, we distinguish two possibilities depending on the value of the imposed pressure gradient. When $G \le G_c$, the standard no-slip solution applies:

$$u_z(r,t) = \frac{R^2 G}{4\eta}\left[1-\left(\frac{r}{R}\right)^2 - 8\sum_{k=1}^{\infty}\frac{1}{\alpha_k^3 J_1(\alpha_k)} J_0\left(\frac{\alpha_k r}{R}\right) e^{-\frac{\alpha_k^2 \nu}{R^2}t}\right], \tag{9}$$

where $J_i$ is the Bessel function of the first kind of order $i$; $\alpha_k$, $k = 1, 2, \ldots$, are the roots of $J_0$; and $\nu \equiv \eta/\rho$ is the kinematic viscosity. Equation (9) is the standard velocity profile with no slip (see (King 2007; Matthews and Hill 2008; Wu et al. 2008; Glasgow 2010). The volumetric flow rate and the wall shear stress are respectively given by

$$Q(t) = \frac{\pi R^4}{8\eta}\left(1 - 32\sum_{k=1}^{\infty}\frac{1}{\alpha_k^4} e^{-\frac{\alpha_k^2 \nu}{R^2}t}\right) G \tag{10}$$

and

$$\tau_w(t) = \frac{R}{2}\left(1 - 4\sum_{k=1}^{\infty}\frac{1}{\alpha_k^2} e^{-\frac{\alpha_k^2 \nu}{R^2}t}\right) G. \tag{11}$$

In the case where $G > G_c$, the no-slip solution applies only up to the critical time $t_c$ at which the wall shear stress becomes equal to the slip yield stress. Hence, for $0 \le t < t_c$, the velocity and the volumetric flow rate are given by Eqs. (9) and (10). The critical time for the initiation of slip, $t_c$, can be found as the root of $\tau_w(t_c) = \tau_c$, i.e. the root of

$$4\sum_{k=1}^{\infty}\frac{1}{\alpha_k^2} e^{-\frac{\alpha_k^2 \nu}{R^2}t_c} = 1 - \frac{2\tau_c}{GR}. \tag{12}$$

It is clear that $t_c$ depends only on the pressure gradient and the slip yield stress. Once $t_c$ is exceeded, $\tau_w > \tau_c$ and slip occurs along the wall following Eq. (5). The solution for the full problem is

$$u_z(r,t) = \begin{cases} \dfrac{R^2 G}{4\eta}\left[1-\left(\dfrac{r}{R}\right)^2 - 8\displaystyle\sum_{k=1}^{\infty}\frac{1}{\alpha_k^3 J_1(\alpha_k)} \times J_0\left(\dfrac{\alpha_k r}{R}\right) e^{-\frac{\alpha_k^2 \nu}{R^2}t}\right], & t \le t_c, \\ \dfrac{R^2 G}{4\eta}\left[1+2B-\left(\dfrac{r}{R}\right)^2 - 4\displaystyle\sum_{n=1}^{\infty} A_n J_0\left(\dfrac{\lambda_n r}{R}\right) \times e^{-\frac{\lambda_n^2 \nu}{R^2}(t-t_c)}\right] - \dfrac{\tau_c B R}{\eta}, & t > t_c, \end{cases} \tag{13}$$

where

$$A_n = \frac{B\left[1+\lambda_n^2 I_n - 2\tau_c/(GR)\right]}{\lambda_n J_1(\lambda_n)\left(1+B^2\lambda_n^2\right)}, \tag{14}$$

$$I_n = 4\sum_{k=1}^{\infty}\frac{1}{\alpha_k^2\left(\alpha_k^2-\lambda_n^2\right)} e^{-\frac{\alpha_k^2 \nu}{R^2}t_c} \tag{15}$$

and $\lambda_n$ are the roots of

$$J_0(\lambda_n) = B\lambda_n J_1(\lambda_n). \tag{16}$$

The volumetric flow rate is given by

$$Q(t) = \begin{cases} \dfrac{\pi R^4}{8\eta}\left[1 - 32\displaystyle\sum_{k=1}^{\infty}\frac{1}{\alpha_k^4} e^{-\frac{\alpha_k^2 \nu}{R^2}t}\right] G, & t \le t_c, \\ \dfrac{\pi R^4}{8\eta}\left[1+4B - 16\displaystyle\sum_{n=1}^{\infty} A_n \frac{J_1(\lambda_n)}{\lambda_n} \times e^{-\frac{\lambda_n^2 \nu}{R^2}(t-t_c)}\right] G - \dfrac{\pi \tau_c B R^3}{\eta}, & t > t_c, \end{cases} \tag{17}$$

and the slip velocity is

$$u_{\mathrm{w}}(t) = \begin{cases} 0, & t \le t_{\mathrm{c}}, \\ \dfrac{R^2 G}{4\eta}\left[2B - 4\displaystyle\sum_{n=1}^{\infty} A_n J_0(\lambda_n) \times e^{-\frac{\lambda_n^2 \nu}{R^2}(t-t_{\mathrm{c}})}\right] - \dfrac{\tau_{\mathrm{c}} B R}{\eta}, & t > t_{\mathrm{c}}. \end{cases} \tag{18}$$

Introducing the following dimensionless quantities

$$u_z^* = \frac{u_z \eta}{\tau_{\mathrm{c}} R}, \quad G^* = \frac{RG}{\tau_{\mathrm{c}}}, \quad \tau^* = \frac{\tau}{\tau_{\mathrm{c}}},$$
$$Q^* = \frac{Q\eta}{\pi \tau_{\mathrm{c}} R^3}, \quad r^* = \frac{r}{R}, \quad t^* = \frac{t\nu}{R^2}, \tag{19}$$

the non-dimensional critical pressure gradient becomes $G_{\mathrm{c}}^* = 2$ and the non-dimensional critical time $t_{\mathrm{c}}^*$ is the solution of

$$4\sum_{k=1}^{\infty} \frac{1}{\alpha_k^2} e^{-\alpha_k^2 t_{\mathrm{c}}^*} = 1 - \frac{2}{G^*}. \tag{20}$$

The non-dimensional velocity and volumetric flow rate are respectively given by

$$u_z^*(r^*, t^*) = \begin{cases} \dfrac{G^*}{4}\left[1 - r^{*2} - 8\displaystyle\sum_{k=1}^{\infty} \frac{1}{\alpha_k^3 J_1(\alpha_k)} J_0\left(\alpha_k r^*\right) e^{-\alpha_k^2 t^*}\right], & t^* \le t_{\mathrm{c}}^*, \\ \dfrac{G^*}{4}\left[1 + 2B - r^{*2} - 4\displaystyle\sum_{n=1}^{\infty} A_n^* J_0(\lambda_n r^*) e^{-\lambda_n^2 (t^* - t_{\mathrm{c}}^*)}\right] - B, & t^* > t_{\mathrm{c}}^*, \end{cases} \tag{21}$$

and

$$Q^*(t^*) = \begin{cases} \dfrac{1}{8}\left[1 - 32\displaystyle\sum_{k=1}^{\infty} \frac{1}{\alpha_k^4} e^{-\alpha_k^2 t^*}\right] G^*, & t^* \le t_{\mathrm{c}}^*, \\ \dfrac{1}{8}\left[1 + 4B - 16\displaystyle\sum_{n=1}^{\infty} A_n^* \frac{J_1(\lambda_n)}{\lambda_n} e^{-\lambda_n^2 (t^* - t_{\mathrm{c}}^*)}\right] G^* - B, & t^* > t_{\mathrm{c}}^*, \end{cases} \tag{22}$$

where

$$A_n^* = \frac{B\left(1 + \lambda_n^2 I_n - 2/G^*\right)}{\lambda_n J_1(\lambda_n)\left(1 + B^2 \lambda_n^2\right)}. \tag{23}$$

Also, the dimensionless slip velocity is given by

$$u_{\mathrm{w}}^*(t^*) = \begin{cases} 0, & t^* \le t_c^* \\ \dfrac{G^*}{2}\left[B - 2\displaystyle\sum_{n=1}^{\infty} A_n^* J_0(\lambda_n) \times e^{-\lambda_n^2 (t^* - t_{\mathrm{c}}^*)}\right] - B, & t^* > t_{\mathrm{c}}^*. \end{cases} \tag{24}$$

In Fig. 1, the critical time $t_{\mathrm{c}}^*$ is plotted as a function of the dimensionless pressure gradient $G^*$. If the pressure gradient is closer to $G_{\mathrm{c}}^* = 2$, it requires a longer time for slip to occur and eventually $t_{\mathrm{c}}^* \to \infty$, while as $G^* \to \infty$, $t_{\mathrm{c}}^* \to 0$ indicating that slip occurs much faster as the pressure gradient increases. As already noted, $t_{\mathrm{c}}^*$ is independent of the slip number $B$. The dashed line denotes an approximation to $t_{\mathrm{c}}^*$, found by retaining only the first them of the sum in Eq. (20):

$$t_{\mathrm{c}}^* \approx \frac{1}{\alpha_1^2} \ln\left[\frac{4G^*}{\alpha_1^2}\left(\frac{1}{G^* - 2}\right)\right]. \tag{25}$$

This approximate value for $t_{\mathrm{c}}^*$ is very close to the actual value, when $G^*$ is close to $G_{\mathrm{c}}^*$, and it breaks down for large values of $G^*$.

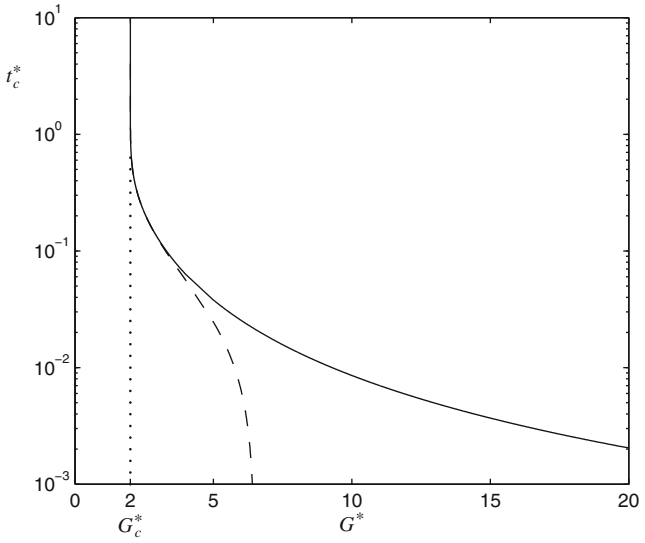


**Fig. 1** The critical time for the initiation of slip, in start-up axisymmetric Poiseuille flow plotted against the dimensionless pressure gradient $G^*$. The *dotted line* represents the critical pressure gradient for the occurrence of slip, $G_c^*$, while the *dashed line* is the first term approximation to $t_c^*$

The dimensionless volumetric flow rate for $G^* = 3$ and various slip numbers is shown in Fig. 2a with the no-slip case denoted by the dashed line. As deduced from Eq. (22), for $t^* \leq t_c^*$, $Q^*$ is independent of the slip number $B$ while for $t^* > t_c^*$, $Q^*$ increases with $B$. It is clear from Fig. 2b, which shows the deviation of $Q^*$ from the steady state dimensionless volumetric flow rate, $Q_s^*$, that the flow requires an infinite time to evolve to steady-state. This is a standard result for Newtonian fluids (Batchelor 1967), while Bingham fluids have been shown to reach steady-state flow in finite time (Glowinski 1984). Additionally, the flow development decelerates as the slip number is increased. This is also seen in Fig. 3 where the evolution of the velocity profile for $G^* = 3$ and three slip numbers ($B = 0.1$, 1 and 10) is illustrated. As the slip number increases, so does the steady-state velocity which tends to become flat for large values of $B$.

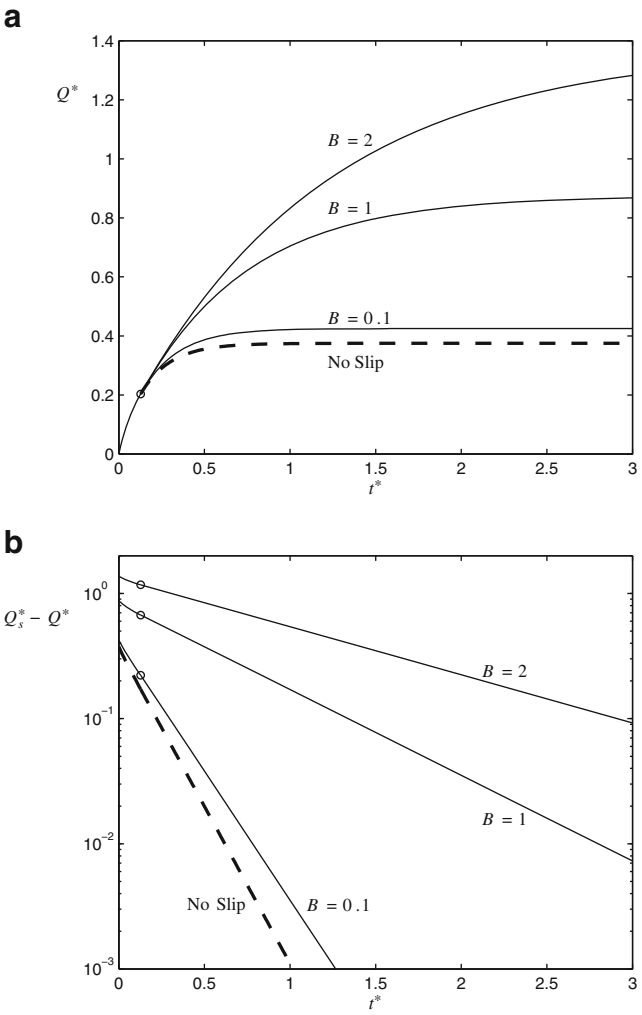


**Fig. 2** Evolution of **a** the dimensionless volumetric flow rate, $Q^*$, and **b** its deviation from the steady-state value in start-up axisymmetric Poiseuille flow for $G^* = 3 > G_c^*$ and various slip numbers $B$. The *dashed line* corresponds to the no-slip case and the *circles* denote the critical time, $t_c$, for the onset of slip

## Plane Poiseuille flow

For completeness, the solution for the start-up plane Poiseuille flow is summarised here. Using similar scalings, i.e.

$$u_x^* = \frac{u_x \eta}{\tau_c H}, \quad G^* = \frac{HG}{\tau_c}, \quad \tau^* = \frac{\tau}{\tau_c},$$
$$Q^* = \frac{Q\eta}{\tau_c H^3}, \quad y^* = \frac{y}{H}, \quad t^* = \frac{t\nu}{H^2}, \tag{26}$$

where $H$ is the slit semi-width, the critical pressure gradient for the occurrence of slip becomes $G_c^* = 1$ and the critical time $t_c^*$ is the solution of

$$2\sum_{k=1}^{\infty} \frac{1}{\alpha_k^2} e^{-\alpha_k^2 t_c^*} = 1 - \frac{1}{G^*}. \tag{27}$$

The non-dimensional velocity is

$$u_x^*(y^*, t^*) = \begin{cases} \dfrac{G^*}{2}\left[1 - y^{*2} - 4\displaystyle\sum_{k=1}^{\infty} \frac{(-1)^{k+1}}{\alpha_k^3} \right. \\ \qquad \left. \times \cos(\alpha_k y^*) e^{-\alpha_k^2 t^*}\right], t^* \leq t_c^*, \\ \dfrac{G^*}{2}\left[1 + 2B - y^{*2} - 4\displaystyle\sum_{n=1}^{\infty} C_n^* \cos(\lambda_n y^*) \right. \\ \qquad \left. \times e^{-\lambda_n^2 (t^* - t_c^*)}\right] - B, t^* > t_c^*, \end{cases} \tag{28}$$

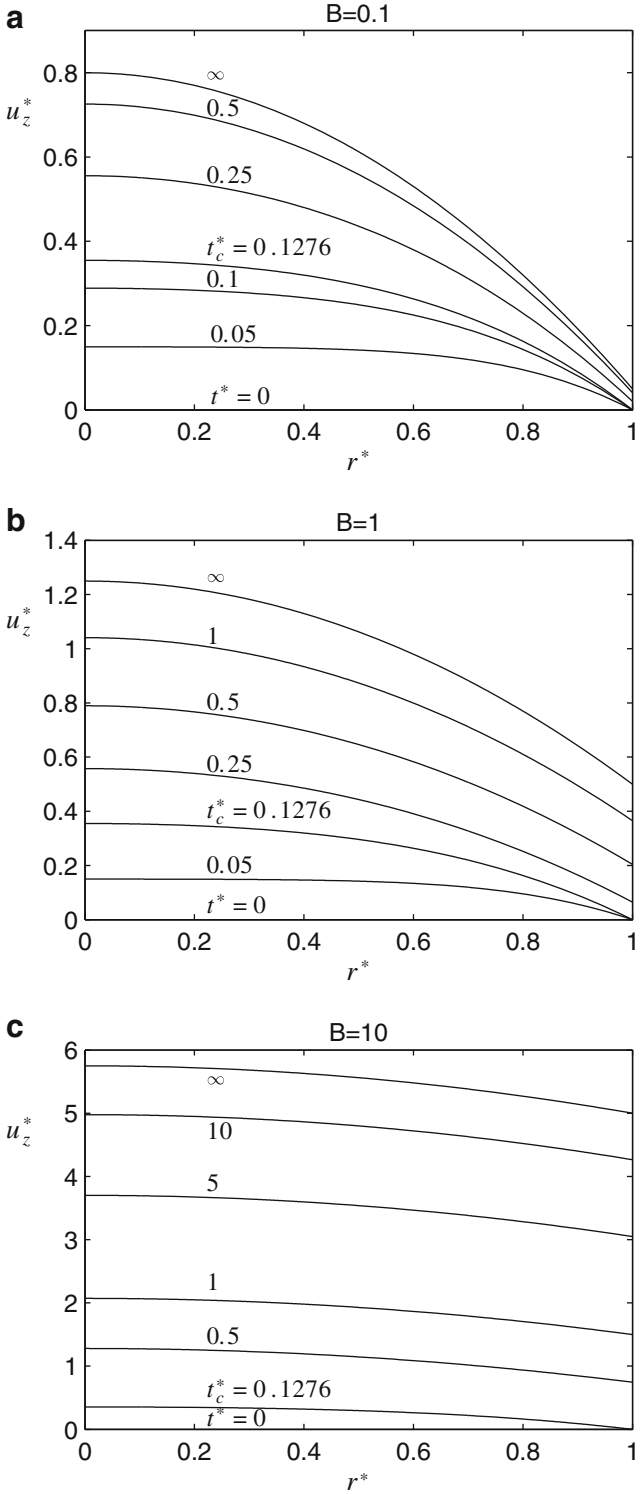


**Fig. 3** Evolution of the velocity in start-up axisymmetric Poiseuille flow for $G^* = 3 > G_c^*$: **a** $B = 0.1$, **b** $B = 1$ and **c** $B = 10$

where

$$C_n^* = \frac{B\left(1+\lambda_n^2 I_n - 1/G^*\right)\sin\lambda_n}{\lambda_n + \sin\lambda_n \cos\lambda_n}, \tag{29}$$

$$I_n = 2\sum_{k=1}^{\infty} \frac{1}{\alpha_k^2\left(\alpha_k^2 - \lambda_n^2\right)} e^{-\frac{\alpha_k^2 \nu}{R^2} t_c}, \tag{30}$$

$\alpha_k = (2k-1)\pi/2$ and $\lambda_n$ are the roots of

$$B\lambda_n \tan\lambda_n = 1, \tag{31}$$

and $B \equiv \eta/(\beta H)$ is the slip number. The non-dimensional volumetric flow rate is

$$Q^*(t^*) \begin{cases} \dfrac{2}{3}\left[1 - 6\displaystyle\sum_{k=1}^{\infty}\frac{1}{\alpha_k^4} e^{-\alpha_k^2 t^*}\right] G^*, & t^* \le t_c^*, \\ \dfrac{2}{3}\left[1 + 3B - 6\displaystyle\sum_{n=1}^{\infty} C_n^* \frac{\sin(\lambda_n)}{\lambda_n} \times e^{-\lambda_n^2 (t^* - t_c^*)}\right] G^* - 2B, & t^* > t_c^*, \end{cases} \tag{32}$$

and the slip velocity is given by

$$u_w^*(t^*) = \begin{cases} \dfrac{G^*}{2}\left[1 - y^{*2} - 4\displaystyle\sum_{k=1}^{\infty}\frac{(-1)^{k+1}}{\alpha_k^3} \times \cos(\alpha_k y^*) e^{-\alpha_k^2 t^*}\right], & t^* \le t_c^*, \\ \dfrac{G^*}{2}\left[1 + 2B - y^{*2} - 4\displaystyle\sum_{n=1}^{\infty} C_n^* \cos(\lambda_n y^*) \times e^{-\lambda_n^2 (t^* - t_c^*)}\right] - B, & t^* > t_c^*. \end{cases} \tag{33}$$

## Annular Poiseuille flow

In this section, we derive solutions for the start-up Newtonian flow in an annular duct of inner and outer radii, $\kappa R$ and $R$, respectively, with $0 < \kappa < 1$. We assume that the properties of the inner and outer walls are the same and denote the corresponding quantities by the subscripts 1 and 2, respectively. Thus, the boundary conditions are given by

$$\left.\begin{array}{ll} u_{w1} = 0, & \tau_{w1} \le \tau_c \\ \eta \left.\dfrac{\partial u_z}{\partial r}\right|_{r=\kappa R} = \tau_c + \beta u_{w1}, & \tau_{w1} > \tau_c \end{array}\right\} \tag{34}$$

and

$$\left.\begin{array}{ll} u_{w2} = 0, & \tau_{w2} \le \tau_c \\ -\eta \left.\dfrac{\partial u_z}{\partial r}\right|_{r=R} = \tau_c + \beta u_{w2}, & \tau_{w2} > \tau_c \end{array}\right\}. \tag{35}$$

As shown in Kaoullas and Georgiou (2013), there are three steady-state flow regimes corresponding to (1) no slip at both walls, (2) slip only at the inner wall and (3) slip at both

walls. These regimes are defined by two critical pressure gradients:

$$G_{c1} = \frac{4\kappa \ln(1/\kappa)\tau_c}{[-2\kappa^2 \ln(1/\kappa) + 1 - \kappa^2]R} \tag{36}$$

and

$$G_{c2} = \frac{4[\ln(1/\kappa) + B(1 + 1/\kappa)]\tau_c}{[2\ln(1/\kappa) + 2B/\kappa(1-\kappa^2) - 1 + \kappa^2]R}, \tag{37}$$

where $G_{c1} < G_{c2}$. The steady-state velocity profile is given by

$$u_z^s(r) = \begin{cases} \dfrac{R^2 G}{4\eta}\left[1 - \left(\dfrac{r}{R}\right)^2 + \dfrac{1-\kappa^2}{\ln(1/\kappa)} \ln\dfrac{r}{R}\right], & G \le G_{c1}, \\ \dfrac{R^2 G}{4\eta}\left[1 - \left(\dfrac{r}{R}\right)^2 + \dfrac{2B\kappa + 1 - \kappa^2 + 4\tau_c B/(GR)}{\ln(1/\kappa) + B/\kappa} \ln\dfrac{r}{R}\right], & G_{c1} < G \le G_{c2}, \\ \dfrac{R^2 G}{4\eta}\left[1 + 2B - \left(\dfrac{r}{R}\right)^2 + \dfrac{2B(1+\kappa) + 1 - \kappa^2}{\ln(1/\kappa) + B(1+1/\kappa)} \left(\ln\dfrac{r}{R} - B\right)\right] - \dfrac{\tau_c B R}{\eta}, & G > G_{c2}, \end{cases} \tag{38}$$

where $B \equiv \eta/(\beta R)$. Thus, depending on the value of the pressure gradient, there are three cases in the start-up flow problem.

If $G \le G_{c1}$, one gets the standard no-slip solution

$$u_z(r,t) = \frac{R^2 G}{4\eta}\left[1 - \left(\frac{r}{R}\right)^2 + \frac{1-\kappa^2}{\ln(1/\kappa)} \ln\frac{r}{R} - 8\sum_{j=1}^{\infty} \frac{1}{\alpha_j^3 [Z_1(\alpha_j) + \kappa Z_1(\kappa\alpha_j)]} Z_0\left(\frac{\alpha_j r}{R}\right) e^{-\frac{\alpha_j^2 \nu}{R^2} t}\right], \tag{39}$$

where

$$Z_i\left(\frac{\alpha_j r}{R}\right) \equiv J_i\left(\frac{\alpha_j r}{R}\right) + \delta_j Y_i\left(\frac{\alpha_j r}{R}\right), \tag{40}$$

$Y_i$ is the Bessel function of the second kind of order $i$ and $\alpha_j$ and $\delta_j$ are the $j$th pair of the roots of

$$Z_0(\alpha_j) = Z_0(\kappa\alpha_j) = 0. \tag{41}$$

The volumetric flow rate is given by

$$Q(t) = \frac{\pi R^4}{8\eta}\left[1 - \kappa^4 - \frac{(1-\kappa^2)^2}{\ln(1/\kappa)} - 32\sum_{j=1}^{\infty} \frac{Z_1(\alpha_j) - \kappa Z_1(\alpha_j)}{\alpha_j^4 [Z_1(\alpha_j) + \kappa Z_1(\kappa\alpha_j)]} e^{-\frac{\alpha_j^2 \nu}{R^2} t}\right] G, \tag{42}$$

while the two wall shear stresses are

$$\tau_{w1}(t) = \frac{R}{4}\left[\frac{1-\kappa^2}{\kappa \ln(1/\kappa)} - 2\kappa + 8\sum_{j=1}^{\infty} \frac{Z_1(\kappa\alpha_j)}{\alpha_j^2 [Z_1(\alpha_j) + \kappa Z_1(\kappa\alpha_j)]} e^{-\frac{\alpha_j^2 \nu}{R^2} t}\right] G \tag{43}$$

and

$$\tau_{w2}(t) = \frac{R}{4}\left[2 - \frac{1-\kappa^2}{\ln(1/\kappa)} - 8\sum_{j=1}^{\infty} \frac{Z_1(\alpha_j)}{\alpha_j^2 [Z_1(\alpha_j) + \kappa Z_1(\kappa\alpha_j)]} e^{-\frac{\alpha_j^2 \nu}{R^2} t}\right] G. \tag{44}$$

When $G > G_{c1}$, no-slip applies only for a finite time interval $0 \le t < t_{c1}$. This critical time value, $t_{c1}$, can be found by demanding that $\tau_{w1}(t_{c1}) = \tau_c$, which leads to

$$8\sum_{j=1}^{\infty} \frac{Z_1(\kappa\alpha_j)}{\alpha_j^2 [Z_1(\alpha_j) + \kappa Z_1(\alpha_j)]} e^{-\frac{\alpha_j^2 \nu}{R^2} t_{c1}} = 2\kappa - \frac{1-\kappa^2}{\kappa \ln(1/\kappa)} + \frac{4\tau_c}{RG}. \tag{45}$$

It is clear that $t_{c1}$ depends only on the pressure gradient and the slip yield stress (i.e. it is independent of $B$). For $t > t_{c1}$, slip occurs along the inner wall.

If $G_{c1} < G \leq G_{c2}$, the flow evolves to the corresponding steady-state without slip at the outer wall. Hence, for $t > t_c$, the velocity is given by

$$u_z(r,t) = \frac{R^2 G}{4\eta}\left[1 - \left(\frac{r}{R}\right)^2 + \frac{2B\kappa + 1 - \kappa^2 + 4\tau_c B/(GR)}{\ln(1/\kappa) + B/\kappa}\ln\frac{r}{R} - 2\sum_{m=1}^{\infty} D_m Z_0\left(\frac{\lambda_m r}{R}\right) e^{-\frac{\lambda_m^2 \nu}{R^2}(t - t_{c1})}\right] \tag{46}$$

where

$$D_m = \frac{B\left[\frac{2\kappa^2\ln(1/\kappa) - 1 + \kappa^2}{\ln(1/\kappa)} + \lambda_m^2 I_m + \frac{4k\tau_c}{GR}\right] Z_1(\kappa\lambda_m)}{\lambda_m\left[Z_1^2(\lambda_m) - \kappa^2\left(1 + \lambda_m^2 B^2\right) Z_1^2(\kappa\lambda_m)\right]}, \tag{47}$$

$$I_m = 8\kappa\sum_{j=1}^{\infty}\frac{Z_1(\kappa\alpha_j)}{\alpha_j^2[Z_1(\alpha_j) + \kappa Z_1(\alpha_j)]\left(\alpha_j^2 - \lambda_m^2\right)} e^{-\frac{\alpha_j^2 \nu}{R^2} t_{c1}}, \tag{48}$$

$$Z_i(\lambda_m r/R) \equiv J_i(\lambda_m r/R) + \epsilon_m Y_i(\lambda_m r/R) \tag{49}$$

and $(\lambda_m, \epsilon_m)$ are the solutions of

$$Z_0(\lambda_m) = Z_0(\kappa\lambda_m) + \lambda_m B Z_1(\kappa\lambda_m) = 0. \tag{50}$$

The volumetric flow rate is given by

$$Q(t) = \frac{\pi R^4}{8\eta}\left[1 - \kappa^4 - \frac{(1-\kappa^2)^2 - N_1}{\ln(1/\kappa) + B/\kappa} - 8\sum_{m=1}^{\infty} D_m \frac{Z_1(\lambda_m) - \kappa Z_1(\kappa\lambda_m)}{\lambda_m} e^{-\frac{\lambda_m^2 \nu}{R^2}(t - t_{c1})}\right] G, \tag{51}$$

where

$$N_1 \equiv 4B\kappa\left[\left(1 + \frac{\tau_c}{GkR}\right)\left[2\kappa^2\ln(1/\kappa) - 1 + \kappa^2\right] - \kappa^2\ln(1/\kappa)\right]. \tag{52}$$

The two wall shear stresses are

$$\tau_{w1}(t) = \frac{R}{4}\left[-2\kappa + \frac{2B\kappa + 1 - \kappa^2 + 4\tau_c B/(GR)}{\kappa[\ln(1/\kappa) + B/\kappa]} + 2\sum_{m=1}^{\infty} D_m \lambda_m Z_1(\kappa\lambda_m) e^{-\frac{\lambda_m^2 \nu}{R^2}(t - t_{c1})}\right] G \tag{53}$$

and

$$\tau_{w2}(t) = \frac{R}{4}\left[2 - \frac{2B\kappa + 1 - \kappa^2 + 4\tau_c B/(GR)}{\ln(1/\kappa) + B/\kappa} - 2\sum_{m=1}^{\infty} D_m \lambda_m Z_1(\lambda_m) e^{-\frac{\lambda_m^2 \nu}{R^2}(t - t_{c1})}\right] G. \tag{54}$$

In the case where $G > G_{c2}$, the velocity profile (46) and the volumetric flow rate (51) are valid only up to a second critical time value, $t_{c2}$, after which $\tau_{wi} > \tau_c$, $i = 1, 2$, and slip occurs along the outer wall too. This second critical time is the solution of $\tau_{w2}(t_{c2}) = \tau_c$, which gives

$$\tau_c = \frac{R}{4}\left[2 - \frac{2B\kappa + 1 - \kappa^2 + 4\tau_c B/(GR)}{\ln(1/\kappa) + B/\kappa} - 2\sum_{m=1}^{\infty} D_m \lambda_m Z_1(\lambda_m) e^{-\frac{\lambda_m^2 \nu}{R^2}(t_{c2} - t_{c1})}\right] G. \tag{55}$$

Clearly, $t_{c2}$ depends on the pressure gradient, the slip yield stress and the slip parameter. Hence, for $t > t_{c2}$, the velocity is given by

$$u_z(r,t) = \frac{R^2 G}{4\eta}\left[1 + 2B - \left(\frac{r}{R}\right)^2 + \frac{2B(1+\kappa) + 1 - \kappa^2}{\ln(1/\kappa) + B + B/\kappa}\left(\ln\frac{r}{R} - B\right) - 2\sum_{n=1}^{\infty} E_n Z_0\left(\frac{\mu_n r}{R}\right) e^{-\frac{\mu_n^2 \nu}{R^2}(t - t_{c2})}\right] - \frac{\tau_c B R}{\eta} \tag{56}$$

where

$$E_n = \frac{B\left[\dfrac{2\ln(1/\kappa)+2B/\kappa-2B\kappa-1+\kappa^2-4\tau_c[\ln(1/\kappa)+B+B/\kappa]/(GR)}{\ln(1/\kappa)+B/\kappa}+\mu_n^2 L_n\right]Z_1(\mu_n)}{\mu_n\left(1+\mu_n^2B^2\right)\left[Z_1^2(\mu_n)-\kappa^2Z_1^2(\kappa\mu_n)\right]}, \tag{57}$$

$$L_n = 2\sum_{m=1}^{\infty} D_m \frac{\lambda_m Z_1(\lambda_m)}{\lambda_m^2-\mu_n^2} e^{-\frac{\lambda_m^2\nu}{R^2}(t_{c2}-t_{c1})}, \tag{58}$$

$Z_i(\mu_n r/R) \equiv J_i(\mu_n r/R)+\phi_n Y_i(\mu_n r/R)$ and the eigenvalues $(\mu_n, \phi_n)$ are the solutions of

$$Z_0(\mu_n) - \mu_n B Z_1(\mu_n) = Z_0(\kappa\mu_n) + \mu_n B Z_1(\kappa\mu_n) = 0. \tag{59}$$

Also, the volumetric flow rate is given by

$$Q(t) = \frac{\pi R^4}{8\eta}\left[1-\kappa^4+4B-\frac{(1-\kappa^2+2B)^2-N_2}{\ln(1/\kappa)+B(1+1/\kappa)}-8\sum_{n=1}^{\infty}E_n\frac{Z_1(\mu_n)-\kappa Z_1(\kappa\mu_n)}{\mu_n}e^{-\frac{\mu_n^2\nu}{R^2}(t-t_{c2})}\right]G - \frac{\pi\tau_c B R^3}{\eta}(1-\kappa^2), \tag{60}$$

where $N_2 \equiv 4B\kappa[\kappa^2\ln(1/\kappa)-1+\kappa^2-2B+B\kappa^2]$. The two wall shear stresses are

$$\tau_{w1}(t) = \frac{R}{4}\left[\frac{2B(1+\kappa)+1-\kappa^2}{\kappa[\ln(1/\kappa)+B(1+1/\kappa)]} -2\kappa+2\sum_{n=1}^{\infty}E_n\mu_n Z_1(\kappa\mu_n)e^{-\frac{\mu_n^2\nu}{R^2}(t-t_{c2})}\right]G, \tag{61}$$

and

$$\tau_{w2}(t) = \frac{R}{4}\left[2-\frac{2B(1+\kappa)+1-\kappa^2}{\ln(1/\kappa)+B(1+1/\kappa)} -2\sum_{n=1}^{\infty}E_n\mu_n Z_1(\mu_n)e^{-\frac{\mu_n^2\nu}{R^2}(t-t_{c2})}\right]G. \tag{62}$$

Using the same scalings as in Eq. (19), the two non-dimensional critical time values are the solutions of

$$8\sum_{j=1}^{\infty}\frac{Z_1(\kappa\alpha_j)}{\alpha_j^2[Z_1(\alpha_j)+\kappa Z_1(\kappa\alpha_j)]}e^{-\alpha_j^2 t_{c1}^*} = 2\kappa-\frac{1-\kappa^2}{\kappa\ln(1/\kappa)}+\frac{4}{G^*} \tag{63}$$

and

$$\sum_{m=1}^{\infty}D_m^*\lambda_m Z_1(\lambda_m)e^{-\lambda_m^2(t_{c2}^*-t_{c1}^*)} = 1-\frac{2B\kappa+1-\kappa^2+4B/G^*}{2[\ln(1/\kappa)+B/\kappa]}-\frac{2}{G^*}, \tag{64}$$

where

$$D_m^* = \frac{B\left[\dfrac{2\kappa^2\ln(1/\kappa)-1+\kappa^2}{\ln(1/\kappa)}+\lambda_m^2 I_m+\dfrac{4k}{G^*}\right]Z_1(\kappa\lambda_m)}{\lambda_m[Z_1^2(\lambda_m)-\kappa^2(1+\lambda_m^2B^2)Z_1^2(\kappa\lambda_m)]}. \tag{65}$$

For $G^* > G_{c2}^*$, the non-dimensional velocity is

$$u_z^*(r^*,t^*) = \begin{cases} \dfrac{G^*}{4}\left[1-r^{*2}+\dfrac{1-\kappa^2}{\ln(1/\kappa)}\ln r^* - 8\sum_{j=1}^{\infty}\dfrac{Z_0(\alpha_j r^*)}{\alpha_j^3[Z_1(\alpha_j)+\kappa Z_1(\kappa\alpha_j)]}e^{-\alpha_j^2 t^*}\right], & t^* \le t_{c1}^*, \\ \dfrac{G^*}{4}\left[1-r^{*2}+\dfrac{2B\kappa+1-\kappa^2+4B/G^*}{\ln(1/\kappa)+B/\kappa}\ln r^* - 2\sum_{m=1}^{\infty}D_m^* Z_0(\lambda_m r^*)e^{-\lambda_m^2(t^*-t_{c1}^*)}\right], & t_{c1}^* < t^* \le t_{c2}^*, \\ \dfrac{G^*}{4}\left[1+2B-r^{*2}+\dfrac{2B(1+\kappa)+1-\kappa^2}{\ln(1/\kappa)+B(1+1/\kappa)}(\ln r^* - B)\right. & \\ \left. -2\sum_{n=1}^{\infty}E_n^* Z_0(\mu_n r^*)e^{-\mu_n^2(t^*-t_{c2}^*)}\right] - B, & t^* > t_{c2}^*, \end{cases} \tag{66}$$

where

$$E_n^* = \frac{B\left[\dfrac{2\ln(1/\kappa)+2B/\kappa-2B\kappa-1+\kappa^2-4[\ln(1/\kappa)+B+B/\kappa]/G^*}{\ln(1/\kappa)+B/\kappa}+\mu_n^2 L_n\right]Z_1(\mu_n)}{\mu_n(1+\mu_n^2B^2)\left[Z_1^2(\mu_n)-\kappa^2Z_1^2(\kappa\mu_n)\right]}. \tag{67}$$

The two non-dimensional slip velocities are given by

$$u_{\mathrm{w1}}^*(t^*) = \begin{cases} 0, & t^* \le t_{\mathrm{c1}}^*, \\ \dfrac{G^*}{4}\left[1-\kappa^2-\dfrac{2B\kappa+1-\kappa^2}{\ln(1/\kappa)+B/\kappa+4B/G^*}\ln(1/\kappa)\right. & \\ \qquad \left.-2\displaystyle\sum_{m=1}^{\infty}D_m^*Z_0(\kappa\lambda_m)e^{-\lambda_m^2(t^*-t_{\mathrm{c1}}^*)}\right], & t_{\mathrm{c1}}^* < t^* \le t_{\mathrm{c2}}^*, \\ \dfrac{G^*}{4}\left[1+2B-\kappa^2-\dfrac{2B(1+\kappa)+1-\kappa^2}{\ln(1/\kappa)+B(1+1/\kappa)}[\ln(1/\kappa)+B]\right. & \\ \qquad \left.-2\displaystyle\sum_{n=1}^{\infty}E_n^*Z_0(\kappa\mu_n)e^{-\mu_n^2(t^*-t_{\mathrm{c2}}^*)}\right]-B, & t^* > t_{\mathrm{c2}}^*, \end{cases} \tag{68}$$

and

$$u_{\mathrm{w2}}^*(t^*) = \begin{cases} 0, & t^* \le t_{\mathrm{c2}}^*, \\ \dfrac{G^*}{4}\left[2B-\dfrac{2B(1+\kappa)+1-\kappa^2}{\ln(1/\kappa)+B(1+1/\kappa)}B-2\displaystyle\sum_{n=1}^{\infty}E_n^*Z_0(\mu_n)e^{-\mu_n^2(t^*-t_{\mathrm{c2}}^*)}\right]-B, & t^* > t_{\mathrm{c2}}^*, \end{cases} \tag{69}$$

and the non-dimensional volumetric flow rate is given by

$$Q^*(t^*) = \begin{cases} \dfrac{1}{8}\left[(1-\kappa^4)-\dfrac{(1-\kappa^2)^2}{\ln(1/\kappa)}-32\displaystyle\sum_{j=1}^{\infty}\frac{Z_1(\alpha_j)-\kappa Z_1(\kappa\alpha_j)}{\alpha_j^4[Z_1(\alpha_j)+\kappa Z_1(\kappa\alpha_j)]}e^{-\alpha_j^2t^*}\right]G^*, & t^* \le t_{\mathrm{c1}}^*, \\ \dfrac{1}{8}\left[(1-\kappa^4)-\dfrac{(1-\kappa^2)^2-N_1^*}{\ln(1/\kappa)+B/\kappa}\right. & \\ \qquad \left.-8\displaystyle\sum_{m=1}^{\infty}D_m^*\frac{Z_1(\lambda_m)-\kappa Z_1(\kappa\lambda_m)}{\lambda_m}e^{-\lambda_m^2(t^*-t_{\mathrm{c1}}^*)}\right]G^*, & t_{\mathrm{c1}}^* < t^* \le t_{\mathrm{c2}}^*, \\ \dfrac{1}{4}\left[1-\kappa^4+4B-\dfrac{(1-\kappa^2+2B)^2-N_2}{\ln(1/\kappa)+B(1+1/\kappa)}\right. & \\ \qquad \left.-8\displaystyle\sum_{n=1}^{\infty}E_n^*\frac{Z_1(\mu_n)-\kappa Z_1(\kappa\mu_n)}{\mu_n}e^{-\mu_n^2(t^*-t_{\mathrm{c2}}^*)}\right]G^*-B(1-\kappa^2), & t^* > t_{\mathrm{c2}}^*, \end{cases} \tag{70}$$

where

$$N_1^* \equiv 4B\kappa\left[\left(1+\frac{1}{G^*k}\right)[2\kappa^2\ln(1/\kappa)-1+\kappa^2]-\kappa^2\ln(1/\kappa)\right]. \tag{71}$$

Figure 4 shows the two critical times, $t_{\mathrm{c1}}^*$ and $t_{\mathrm{c2}}^*$, at various pressure gradients, $\kappa = 0.1$ and $B = 0.001$, $B = 1$ and $B \to \infty$. The first critical time depends only on the pressure gradient, while the second one depends on both the pressure gradient and the slip number. As expected, both $t_{\mathrm{c1}}^*$ and $t_{\mathrm{c2}}^*$

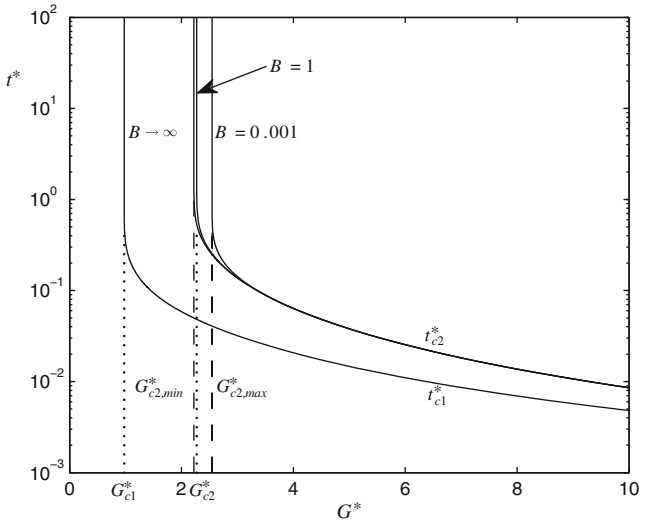


**Fig. 4** The two critical times, $t^*_{c1}$ and $t^*_{c2}$, for the initiation of slip at the inner and outer walls, respectively, in start-up annular Poiseuille flow with $\kappa = 0.1$ and different values of the slip number. The *dotted lines* represent the two critical pressure gradients, $G^*_{c1}$ and $G^*_{c2}$, while the maximum and minimum values of the latter are indicated by the *dashed lines*

tend to infinity as $G^* \to G^*_{c1}$ and $G^* \to G^*_{c2}$, respectively. Also both critical times tend to zero as $G^* \to \infty$; thus, slip occurs much quicker. Unlike $G^*_{c1}$, $G^*_{c2}$ depends on $B$ and is bounded by $G^*_{c2,min} \le G^*_{c2} \le G^*_{c2,max}$, where

$$G^*_{c2,min} \equiv \lim_{B\to\infty} G^*_{c2} = \frac{2}{1-\kappa} \tag{72}$$

and

$$G^*_{c2,max} \equiv \lim_{B\to 0} G^*_{c2} = \frac{4\ln(1/\kappa)}{2\ln(1/\kappa) - 1 + \kappa^2}. \tag{73}$$

Hence, for $\kappa = 0.1$, $G^*_{c2,min} = 2.2222$ and $G^*_{c2,max} = 2.5477$.

Figure 5a shows the non-dimensional volumetric flow rate for different slip numbers with the no-slip case denoted by the dashed line. The left branch corresponds to the no-slip stage of the flow. The middle branch begins at $t^*_{c1}$ (circles), which is the same for all $B$ and corresponds to slip only at the inner wall, while the upper branch begins at $t^*_{c2}$ (dots), which is different for each $B$ and corresponds to the slip-at-both-walls case. For both the middle and upper branches, $Q^*$ increases with increasing $B$. It can be seen in Fig. 5b, which shows the deviation of $Q^*$ from the steady-state value, that the flow development decelerates with increasing $B$ and that the flow requires an infinite time to reach a steady state. The evolution of the velocity for $\kappa = 0.1$, $G^* = 2.6$ and three slip numbers ($B = 0.001$, 1 and 1,000) is illustrated in Fig. 6. As in the axisymmetric and planar flows, the velocity also increases with $B$ and eventually becomes flat. Finally, Fig. 7 shows the evolution

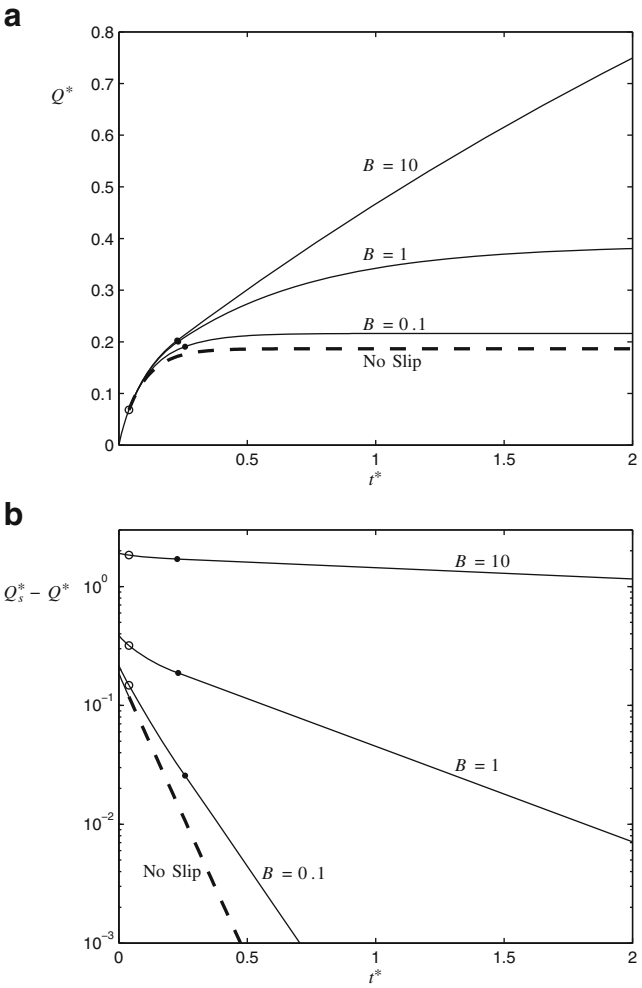


**Fig. 5** **a** The dimensionless volumetric flow rate, $Q^*$, and **b** its deviation from the steady-state value in the annular Poiseuille flow with $\kappa = 0.1$, $G^* = 2.6$ and different slip numbers. The *dashed line* corresponds to the no-slip case, and the critical times for the onset of slip at the inner and outer walls, $t^*_{c1}$ (*circles*) and $t^*_{c2}$ (*dots*), are also noted

of the two slip velocities for $\kappa = 0.1$, $G^* = 2.6$ and two slip values ($B = 0.1$ and 1).

## Conclusions

Analytical solutions of the start-up incompressible Newtonian Poiseuille flows are presented, for the axisymmetric, planar and annular geometries. The slip model employed here allows for slip to occur along the walls only when the wall shear stress exceeds the slip yield stress. In the case of planar and axisymmetric flows, if the imposed pressure gradient is lower than the critical pressure gradient for the occurrence of slip, one gets the classical, transient, no-slip solutions. Otherwise, the no-slip condition applies only up to a critical time, which depends on the slip yield stress and

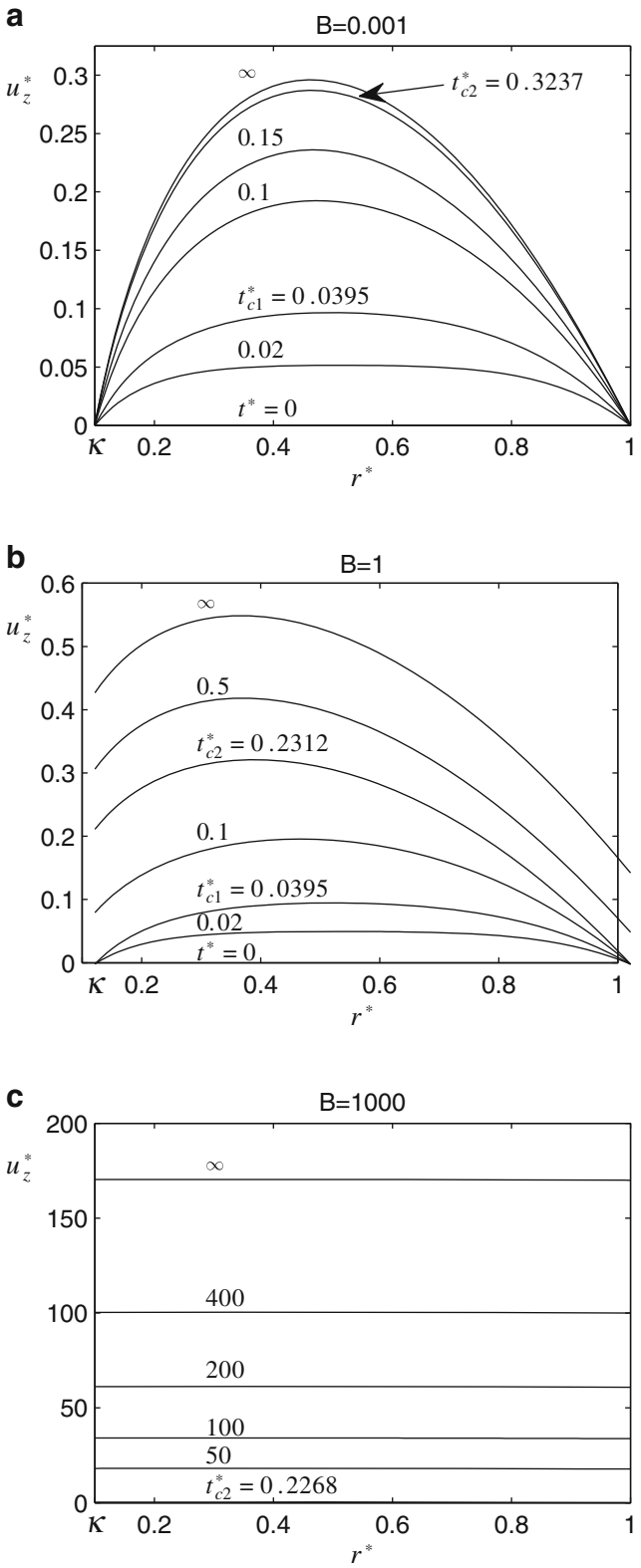


**Fig. 6** Evolution of the velocity profile in start-up annular Poiseuille flow with $\kappa = 0.1$, $G^* = 2.6$ and different values of the slip number: **a** $B = 0.001$, **b** $B = 1$ and **c** $B = 1{,}000$

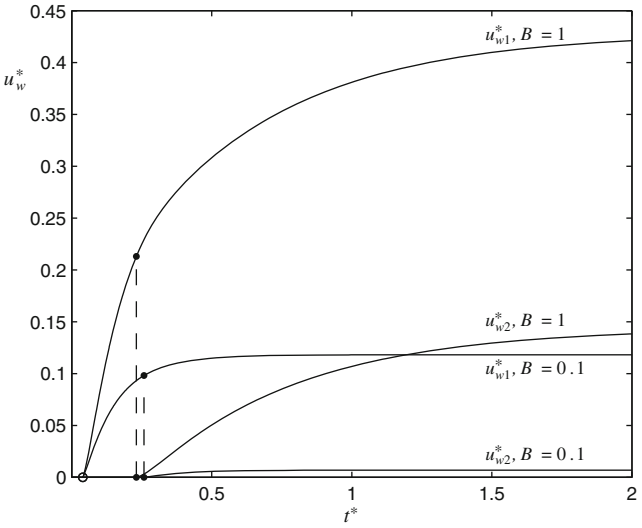


**Fig. 7** Evolution of the two slip velocities, $u_{w1}^*$ and $u_{w2}^*$, in start-up annular Poiseuille flow with $\kappa = 0.1$, $G^* = 2.6$ and $B = 0.1$ and $B = 1$. The critical times for the onset of slip at the inner and outer walls, $t_{c1}^*$ (*circle*) and $t_{c2}^*$ (*dots*), are also noted

the pressure gradient, beyond which the slip yield stress is exceeded and slip does occur.

In the annular flow, the velocity may evolve from no slip at both walls to slip at the inner wall only, and eventually to slip at both walls depending on the value of the applied pressure gradient. These transitions occur when the wall shear stress exceeds the slip yield stress, first at the inner wall and then at the outer wall.

## References

Ansari M, Inn YW, Sukhadia AM, DesLauriers PJ, Hatzikiriakos SG (2013) Wall slip of HDPEs: molecular weight and molecular weight distribution effects. J Rheol 57(3):927–948

Aral BK, Kalyon DM (1994) Effects of temperature and surface roughness on time-dependent development of wall slip in steady torsional flow of concentrated suspensions. J Rheol 38(4):957–972

Ballesta P, Petekidis G, Isa L, Poon WCK, Besseling R (2012) Wall slip and flow of concentrated hard-sphere colloidal suspensions. J Rheol 56:1005–1037

Barnes HA (1995) A review of the slip (wall depletion) of polymer solutions, emulsions and particle suspensions in viscometers: its cause, character, and cure. J Non-Newtonian Fluid Mech 56(3):221–251

Batchelor GK (1967) An introduction to fluid dynamics. Cambridge University Press, Cambridge

Chatzimina M, Georgiou GC, Housiadas K, Hatzikiriakos SG (2009) Stability of the annular Poiseuille flow of a Newtonian liquid with slip along the walls. J Non-Newtonian Fluid Mech 159:1–9

Choo JH, Glovnea RP, Forrest AK, Spikes HA (2007) A low friction bearing based on liquid slip at the wall. J Tribol 129(3):611–620

Craig VSJ, Neto C, Williams DRM (2001) Shear-dependent boundary slip in an aqueous Newtonian liquid. Phys Rev Lett 87:054504
Denn MM (2001) Extrusion instabilities and wall slip. Ann Rev Fluid Mech 33:265–287
Duan ZP, Muzychka YS (2007a) Slip flow in elliptic microchannels. Int J Therm Sci 46(11):1104–1111
Duan ZP, Muzychka YS (2007b) Slip flow in non-circular microchannels. Microfluid Nanofluid 3(4):473–484
Ebert WA, Sparrow EM (1965) Slip flow in rectangular and annular ducts. J Basic Eng 87(4):1018–1024
Estellè P, Lanos C (2007) Squeeze flow of Bingham fluids under slip with friction boundary condition. Rheol Acta 46:397–404
Ferrás LL, Nóbrega JM, Pinho FT (2012) Analytical solutions for Newtonian and inelastic non-Newtonian flows with wall slip. J Non-Newtonian Fluid Mech 175–176:76–88
Glasgow LA (2010) Transport phenomena: an introduction to advanced topics. Wiley, Hoboken
Glowinski R (1984) Numerical methods for nonlinear variational problems. Springer, New York
Hatzikiriakos SG (2012) Wall slip of molten polymers. Prog Polym Sci 37(4):624–643
Hatzikiriakos SG, Dealy JM (1991) Wall slip of molten high density polyethylene. I. Sliding plate rheometer studies. J Rheol 35(4):497–523
Kalika DS, Denn MM (1987) Wall slip and extrudate distortion in linear low-density polyethylene. J Rheol 31(8):815–834
Kalyon DM, Gevgilili H (2003) Wall slip and extrudate distortion of three polymer melts. J Rheol 47(3):683–699
Kaoullas G, Georgiou GC (2013) Newtonian Poiseuille flows with slip and non-zero slip yield stress. J Non-Newtonian Fluid Mech 197:24–30
King MR (2007) Oscillatory gas flow in a circular nanotube. Open Nanosci J 1(1):1–4
Majdalani J (2008) Exact Navier-Stokes solution for pulsatory viscous channel flow with arbitrary pressure gradient. J Propuls Power 24(6):1412–1423
Matthews MT, Hill JM (2008) Nanofluidics and the Navier boundary condition. Int J Nanotechnol 5(2/3):218–242
Navier CLMH (1827) Sur les lois de mouvement des fluides. Mem Acad R Sci Inst Fr 6:289–440
Neto C, Craig VSJ, Williams DRM (2003) Evidence of shear-dependent boundary slip in Newtonian liquids. Eur Phys J E 12:71–74
Neto C, Evans DR, Bonaccurso E, Butt HJ, Craig VSJ (2005) Boundary slip in Newtonian liquids: a review of experimental studies. Rep Progr Phys 68(12):2859–2897
Spikes H, Granick S (2003) Equation for slip of simple liquids at smooth solid surfaces. Langmuir 19:5065–5071
Tang HS, Kalyon DM (2008a) Time-dependent tube flow of compressible suspensions subject to pressure dependent wall slip: ramifications on development of flow instabilities. J Rheol 52(5):1069–1090
Tang HS, Kalyon DM (2008b) Unsteady circular tube flow of compressible polymeric liquids subject to pressure-dependent wall slip. J Rheol 52(2):507–525
Wiwatanapataphee B, Wu YH, Hu M, Chayantrakom K (2009) A study of transient flows of Newtonian fluids through micro-annuals with a slip boundary. J Phys A: Math Theor 42(6):065,206
Wu YH, Wiwatanapataphee B, Hu M (2008) Pressure-driven transient flows of Newtonian fluids through microtubes with slip boundary. Phys A: Stat Mech Appl 387(24):5979–5990
Zhu Y, Granick S (2001) Rate-dependent slip of Newtonian liquid at smooth surfaces. Phys Rev Lett 87(9):096,105
Zhu Y, Granick S (2002) No-slip boundary condition switches to partial slip when fluid contains surfactant. Langmuir 18(26):10,058–10,063